Continuum analysis to assess field enhancements for tailoring electroporation driven by monopolar or bipolar pulsing based on nonuniformly distributed nanoparticles

Q. Hu[1] and R. P. Joshi [2,*]

[1]*School of Engineering, Eastern Michigan University, Ypsilanti, Michigan 48197, USA*
[2]*Department of Electrical and Computer Engineering, Texas Tech University, Lubbock, Texas 79409, USA*

Recent reports indicate that nanoparticle (NP) clusters near cell membranes could enhance local electric fields, leading to heightened electroporation. This aspect is quantitatively analyzed through numerical simulations whereby time dependent transmembrane potentials are first obtained on the basis of a distributed circuit mode, and the results then used to calculate pore distributions from continuum Smoluchowski theory. For completeness, both monopolar and bipolar nanosecond-range pulse responses are presented and discussed. Our results show strong increases in TMP with the presence of multiple NP clusters and demonstrate that enhanced poration could be possible even over sites far away from the poles at the short pulsing regime. Furthermore, our results demonstrate that nonuniform distributions would work to enable poration at regions far away from the poles. The NP clusters could thus act as distributed electrodes. Our results were roughly in line with recent experimental observations.

I. INTRODUCTION

Electric fields have been used for cell fusion [1,2], electrorotation [3,4], dielectrophoresis [5,6], and separation of cancer cells [7,8]. Applications of electric pulses can also be used to create pores in biological cell membranes leading to orders-of-magnitude increase in plasma membrane permeability and have many interesting biomedical applications [9–17]. Early on, Neumann and colleagues [18] used pulsed electric fields to temporarily permeabilize cell and coined the term "electroporation." Since then rapid advances have been made, with more recent applications including gene electrotransfer [19,20], delivery of plasmid DNA and other exogenous molecules into cells [20–25], electrochemotherapy [26,27], drug delivery [28,29], and controlled immunotherapy [30–32]. As a nonviral method, electrotransfection has benefits of low cost, ease and safety, and independence of cell surface receptors. It is also capable of delivering a wide spectrum of genes with different sizes. An especially important application is that of electrochemotherapy [33–36], defined as the local potentiation by means of electric pulses, towards cancer treatment [37,38]. When the principle of electroporation is combined with certain chemotherapeutic drugs, the cytotoxicity of these drugs is increased tenfold (or higher), leading to improved and dramatic responses in the target tumors. This is called electrochemotherapy [35–38], defined as the local potentiation by means of electric pulses.

Recent developments involve the use of high intensity ($\sim$50–100 kV/cm), nanosecond duration pulsed electric fields [15,39,40]. Potential applications include electrically triggered intracellular calcium release [41,42], shrinkage of

tumors [43,44], temporary blockage of action potential in nerves [45], and activation of platelets for accelerated wound healing [46]. Moderate intensity electric pulses in the microsecond regime is another emerging modality for relatively safe, effective, and minimally invasive ablation [47]. The nonthermal nature of this excitation (unlike the heating caused by microwave or radiofrequency ablation) allows for treatment even in close proximity to critical structures and/or large vessels and mitigates muscle contractions [48,49]. Eliminating contractions helps improve the procedural safety of patients, since the need for neuroparalytic drugs to inhibit muscle contraction is then virtually eliminated. The short duration also eliminates localized thermal heating. Significant progress in this field, based on irreversible electroporation and bipolar high-frequency pulses, has been shown by the Davalos group [50,51].

The electroporation-based methods for drug delivery and therapies have usually relied on contacted techniques such as either plate or needle electrodes inserted into tissue. However, an electroporative system based on direct electrodes alone has a number of drawbacks. For example, the electric field distribution at the sample depends on the dielectric environment and cannot easily be changed or tailored [52,53]. Hence, not all areas that need treatment might attain the requisite field exposure levels, while other spots might develop excessively high fields leading to local heating and collateral damage. Also, regions of high electric fields can promote electrochemical reactions at the electrode-liquid interface and release metallic ions. For example, if ions are introduced, an undesirable outcome can be the biochemical conversion of inositol phosphates into a form that catalyzes release of excess Ca^{2+}, thereby disturbing intracellular signaling [54]. In addition, metal ions can interact with various nucleic acids and proteins, causing them to precipitate from solutions [55,56],

---

*Corresponding author: ravi.joshi@ttu.edu

thus reducing the availability of pDNA for cell transfection. The rapid falloff in fields, on the other hand, implies electroporation over regions further away from the electrodes would be weak or nonexistent. It is, therefore, important to attain an optimum yet well-directed distribution of the external fields for maximal efficiency, drug delivery, and electrochemo treatments.

As was reported some years ago, the application of electrical fields in multiple directions can lead to increased electrotransfer, plasmid uptake, and gene expression [57–59]. This approach was shown to permeabilize a greater area of the cell surface and a larger number of cells in target tissue regions [60]. Such a directional targeting strategy could achieve a twofold outcome: (i) tailor the field distribution for greater coverage of the target tissue regions at requisite field levels without exceeding limits of breakdown or fostering localized thermal heating, and (ii) facilitate selective field enhancements as desired.

A similar idea in this regard was the addition of highly conductive gold nanoparticles which demonstrated enhanced electroporation performance to yield stronger and more efficient DNA delivery in mammalian cells [61]. Initial applications of nanoparticles (NPs) in the field of medicine traditionally focused on their use as contrast agents for medical imaging [62–64]. The physical properties of certain NPs have also been used as radioenhancement agents [65], or to treat cancer by photothermal therapy wherein NPs are used to absorb near-infrared light to kill cancer cells by the heat generated from the incident illumination [66]. Local electric field enhancements leading to significant cellular permeabilization through distributed nanoelectrodes in the form of conductive gold NPs close to the membrane have recently been reported [67]. These findings open up an avenue for noninvasive, smart drug delivery and drug nanocarrier applications [68,69]. Furthermore, the use of NPs would ensure local perturbations and membrane porations over nanoscale regions without affecting the entire membrane or causing collateral damage. For example, in the case of excitable cells which have embedded sodium and potassium pumps, the NP-assisted poration might avoid triggering or damaging the channels, while selectively affecting only the pump-free membrane regions. Experimental data look promising, and have demonstrated the increase in the number of electroporated cells and underscored the potential of conductive NPs in enhancing electroporation efficiency.

Here, our primary focus is on predictions of the transmembrane potential (TMP) buildup in a spherical cell in response to nanosecond electrical pulses in the presence of metallic NPs in close proximity. It has recently been shown that the use of separate, longer duration, electric pulses can help bring the NPs closer to the cell membrane based on electrophoretic force drivers [70]. Hence, the close proximity requirement could be engineered. Here, the TMP is calculated based on a distributed circuit model as discussed elsewhere [15,71,72] which is equivalent to a time-domain nodal analysis. The role of the NPs in modifying and enhancing the TMP is probed with regard to its position and the distance from the membrane, and orientation. The results from the time-evolving TMP are fed into a continuum Smoluchowski equation [73–75] for analysis of pore formation, growth, and decay. The use of NPs for local amplification of electric fields

were recently discussed [76], and experimental data seem to show benefits [77]. This contribution attempts to provide a simulation-based study in this regard, and our results qualitatively support the recent findings. In addition to monopolar pulsing, the present simulations also include comparisons of cellular responses to bipolar excitation in the presence of NP clusters.

II. ELECTROPORATION MODELING DETAILS

The physics of electroporation and the related mechanistic details remains elusive. The overall process is the likely consequence of structural rearrangement of membrane lipids, or lipidic chemical modifications, functional modulation of membrane proteins, or a combination thereof. From a simple electrostatic standpoint, a spatially nonuniform external field acting at the sites of the molecular dipoles within the membrane lipids likely initiates torques and driving forces that move the headgroups. This allows water entry, and the hydrophobic interaction between water and the lipid interior then works to create pores with the hydrophobic lipid tails structurally rearranged to elude the penetrating water channels. While electroporation is driven by an applied electric field, it is not strictly a threshold event requiring a minima field magnitude. In fact, the mean pore creation times can range from ~1 ns to over a few seconds [78,79], depending on the transmembrane potential (TMP). The TMP is typically in the range of 0.2 V to over 1 V depending on the cell type [80]. Here, a simple analysis is used to compute the TMP due to the distributed electric field, which subsequently drives pore creation.

A. Transmembrane potential

Our approach for calculating the transmembrane potential is based on a time-domain nodal analysis involving a distributed equivalent circuit representation of a cell and its membrane structures based on a three-dimensional spatial structure. The dynamic electric field in the simulation region can then be obtained from the node voltages. Details of this method and its implementation have been given elsewhere [15,71] and hence, only a brief outline will be discussed here. Essentially, the entire cell volume was broken up into finite segments, and each segment represented by a parallel resistive-capacitive (RC) combination to account for the current flow and charging effects. Here, the computational region was taken to be a sphere that included the cell with its outer membrane, the aqueous intracellular medium, and surrounding suspension, discretized along the r, θ, and φ directions. For simplicity, the cell membrane itself was taken as an integral unit in this r direction, i.e., this subregion was not further discretized. For interior nodes, the current continuity equation is of the form

$$\sum_{k=1}^{6} \left(\sigma E + \varepsilon \frac{\partial E}{\partial t} \right)_k \times A_k = \sum_{k=1}^{6} I_k = 0, \qquad (1)$$

where I_k are currents along the six faces of an elemental cube with surface areas A_k, the local electric field is E, while ε and σ are the average permittivity and conductivity at the site of each cube. The presence of NP clusters were included by

modifying the local conductivities (to 4.5×10^7 S/m for gold) appropriately at the relevant grid points.

Combining the current continuity then leads to N equations for the N unknown node voltages which can be solved using matrix decomposition techniques. Potentials on each node were updated at every time step based on the boundary conditions imposed by the externally applied field, and the dynamic membrane conductivity which changes over time due to electroporation. Nodes on the periphery of the simulation region of radius R were assigned potential values as boundary conditions in keeping with the external electric fields. For example, for an external field of magnitude E_0 directed along the z direction, the boundary nodes were set to values of $-E_0 R \cos(\theta)$, with θ being the angular location of the node relative to the z axis.

The NP clusters were treated as perfect conductors with no electric field inside their volume. For simplicity, the spatial extent of individual NP cluster was taken to be in units of the elemental volume $r^2 \sin(\theta)\, dr\, d\theta\, d\phi$. The NP clusters were placed close to the cell membrane (i.e., $r \sim R$, the cell radius), but varied in their angular placement. In addition, multiple NPs were also positioned to probe the outcomes and collective or synergistic effects, if any. However, use of elemental volume on the basis of the spherical grid implies that the NP volume placed around the cell in these simulations depended on $\sin(\theta)$, and so was progressively larger moving towards the equator (at $\theta = 90°$).

It must be mentioned for completeness that constant permittivity values (i.e., independent of time and spatial position) were used for both the membrane and the aqueous medium. However, quite conceivably, the high fields created by the nanoparticles could lead to spatial changes in permittivity with formation of double layers as reported [81,82]. The enhanced field created by the presence of locally distributed nanoparticles acting on the presence of dipolar (zwitterionic) lipid headgroups can lead to orientational changes and ordering of the water dipoles, cause excluded volume effects, and reduce the permittivity based on the local electric field strength [83]. However, the field strengths at which the permittivity starts to reduce is about 10^8 V/m as seen in Fig. 4 of Ref. [83]. Here in the present simulation, the applied electric field was 60 kV/cm. So even assuming a tenfold amplification in the local field, the strength would be enhanced to only about 6×10^7 V/m field. Hence, ignoring permittivity changes seem reasonable. In any case, though these effects merit deeper analyses, they are beyond the present scope.

B. Membrane nanopores based on Smoluchowski continuum analysis

Pore generation, growth, and size-evolution required to characterize time-dependent membrane conductivity were obtained based on the Smoluchowski continuum theory [74,84–87]. Smoluchowski theory hinges on the notion of random walks of the pore radius in "r space." Fluctuations in pore radius ("r") arise from the constant entry and egress of water and the constant motion of the lipid molecules. The concept of using a diffusive motion (which is a manifestation of the probabilistic Brownian motion) across an energy landscape was originally proposed in 1916 [88], reviewed by Chandrasekhar

TABLE I. Simulation parameters used.

Pulse types	Monopolar and bipolar
Pulse rise time	1.5 ns
Pulse fall time	1.5 ns
Membrane permittivity	$4 \times 8.85 \times 10^{-12}$ F/m
Membrane conductivity	5.3×10^{-6} S/m
Membrane thickness	5 nm
Cell radius	2.2 microns
Grid points R direction	42 grid points
Grid points Θ direction $(0–\pi/2)$	21 grid points
Grid points Φ direction $(0–2\pi)$	20 grid points

[89], and subsequently used by Kramers to develop the theory of activated transition rates in the limit of large friction [90]. As a consequence of the fluctuating-dissipative nature of the biosystem, the evolution of the mechanical variables (the pore density in this case) can also be expected to follow a diffusive Brownian motion across the energy landscape. The electric field obtained from the calculations discussed in the previous section were the drivers for the poration. Here the full Smoluchowski model was solved, rather than using the asymptotic approximation of Neu and Krassowska [74]. This enabled calculations of the time-dependent pore density $N(r,\theta,\varphi,t)$ at different locations on the membrane surface. Table I lists the parameter values used in the present simulation work. The thickness given in Table I pertains to the lipid bilayer. Other biological details such as the presence of a cytoskeleton, glycocalyx, etc., have been ignored. More details of our transport model can be found elsewhere [91].

III. SIMULATION RESULTS AND DISCUSSION

Simulations for the transmembrane potential (TMP) were carried out first. The TMP values as a function of time for a spherical cell without any nanoparticles for various points on the membrane surface were obtained as a starting baseline. Results for the TMP at eight different angular locations θ around the cell are shown in Fig. 1. Electroporation was taken into account. The applied pulse was chosen to have a maximum electric field amplitude of 60 kV/cm, with rise and fall times of 1.5 ns and an ON time of 70 ns. These pulse characteristics were used in the simulations presented. The pulse duration assumed here perhaps deserves some comment and clarification. While electroporation does require an external electric field to drive the process, there is no set threshold value for the field magnitude. A lower field can lead to electroporation, though the time for pore formation would correspondingly then be much longer. Reports in the literature, for example, based on both observed data [79] and modeling [78], have shown that mean pore creation times could span a large range from a few nanoseconds to over a few seconds. The corresponding transmembrane potentials would then be in the range of 0.2 V to over 1.0 V. Similarly, molecular dynamics simulations [92–94] have shown nanopore formation to occur within a few nanoseconds at high electric field levels. From a practical standpoint, it has been demonstrated that calcium bursts in human lymphocytes can
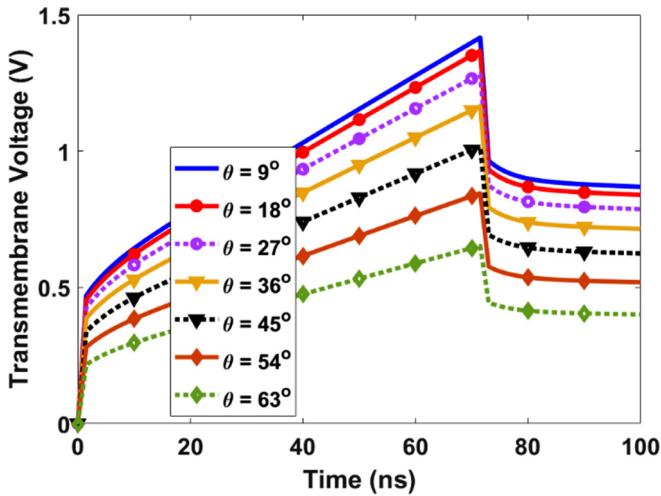
FIG. 1. Transmembrane potential (TMP) as a function of time for a spherical cell at eight different angular locations without any nanoparticles. Electroporation as taken into account for a pulse with maximum electric field amplitude of 60 kV/cm, rise and fall times of 1.5 ns, and an ON time of 70 ns.

FIG. 2. Simulation results for the TMP as a function of time for one nanoparticle (NP) cluster located close to the cell membrane over the $9° < \theta < 18°$ segment. The TMP values at seven different angular locations are shown. The $\theta = 18°$ location shows a drop in the TMP after about 50 ns, indicating a membrane poration.

be triggered by ultrashort electric field pulses of less than 30 ns duration, at fields around 10 kV/cm [95]. This is important, since it shows poration with such ultrashort pulse durations to be possible. Hence, our use of a 70-ns pulse duration is a reasonable choice, especially since short pulses are known to better penetrate cells [96].

In all cases, the TMP is seen to rise in Fig. 1 throughout the pulse duration at all seven locations, signifying a lack of poration. A poration event would have triggered a voltage collapse, and a decrease in the transmembrane potential. In the various curves, a fast initial TMP rise over the first 2-ns interval is seen, with continued increases throughout the pulse, though at a slower rate. The highest magnitudes occur close to the poles (small θ angles), with reductions in TMP as the angular deviation is increased. Upon pulse termination the TMP drops sharply, followed by a very slow falloff that appears almost flat. Since the membrane is not porated in this case, the membrane resistance (R) remains high, effectively leading to a large RC time constant and very slow discharge times. The TMP values are all predicted to remain nearly unchanged up to the maximum 100-ns simulation time.

Simulation results for the TMP as a function of time with one NP cluster were obtained next. In this first set of results (as with other simulations), the NP cluster was taken to be located 50 nm from the cell membrane over the $9° < \theta < 18°$ angular segment. In all the simulations discussed here, each NP cluster was taken to be 346 nm in extent along the θ direction, with a 50-nm span in the r direction. Hence, the effective dimension L of any NP cluster [with $L^3 = r^2\sin(\theta)drd\theta d\phi$] located at an angular position θ, based on the values given in Table I, was $L = 156[\sin(\theta)]^{1/3}$ nm. Given that large NP can be fabricated, and that the functionalization increases their size even further, the current values chosen are roughly in an acceptable range. Also, the distance of the NPs from the membrane for any angular position was always taken to be 50 nm in these simulations. The TMP values obtained at seven different angular locations are shown in Fig. 2. The highest
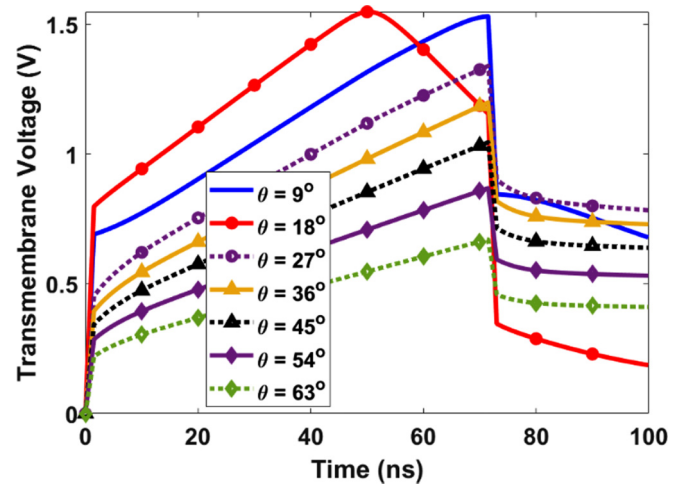
values are predicted to be ∼1.5 V at the $\theta = 9°$ and $18°$ positions. A drop in the TMP is seen to occur at the $\theta = 18°$ location after about 50 ns indicating a membrane poration event, while the other six curves show no voltage decrease throughout the pulse duration. Since the NP cluster was taken to lie between the $9° < \theta < 18°$ angular segment, the electric fields were modified in this vicinity, and led to pore formation at the $\theta = 18°$ location. The interesting outcome is that despite being closer to the pole, neither the $\theta = 9°$ location, nor the $\theta = 0°$ position (result not shown) were predicted to porate. Also, as might be expected, the TMP falloff and recovery after pulse termination is the fastest at the $\theta = 18°$ location due to a smaller membrane resistance locally.

Carrying on, a single NP cluster was taken to again be 50 nm from the cell membrane, but spread over the $45° < \theta < 54°$ angular segment. The simulation results for the TMP are shown in Fig. 3 as a function of time. The values have been given for the same seven angular locations shown in Fig. 2. In this case, the $\theta = 54°$ location is seen to exhibit a drop in the TMP after about 45 ns, indicating membrane poration over that region. Following pulse termination, the TMP at the $54°$ angular location is predicted to drop to near zero voltage levels due to the sharply negative displacement current during pulse turnoff. With a relatively small TMP build up during the ON phase due to the large angular position, the dropoff takes the TMP to a near zero level. In any event, the present results are similar to the previous case in that a pore is predicted to form near the site of a NP cluster, but over the region relatively further from the pole. The other locations of $\theta = 9°, 18°, 27°, 36°$, and $45°$ are all predicted to remain unporated despite being closer to the pole. This suggests that it would be possible to porate cellular areas lying further towards the equator through suitable placement of NP clusters. This central result is in keeping with the observations of the French group [70,77].

In order to test the possibility of forcing poration through suitable placement of nanoparticles, simulations were next
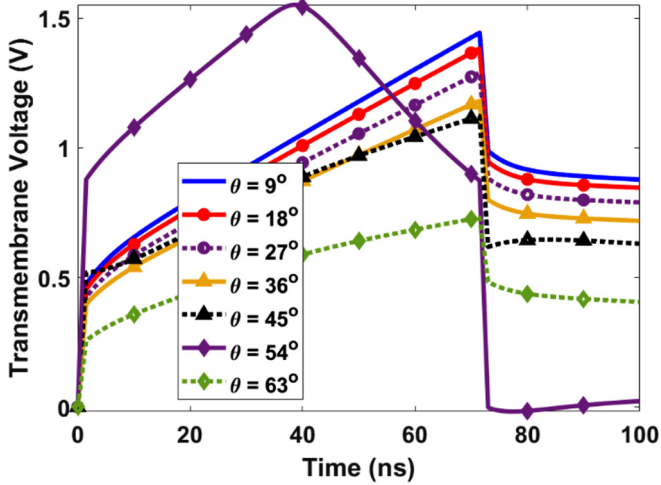
FIG. 3. Simulation results for the TMP as a function of time for one NP cluster located close to the cell membrane over the $45° < \theta < 54°$ angular segment. The TMP values at the same seven angular locations as given in Fig. 2 are shown. The $\theta = 54°$ location shows a drop in the TMP after about 45 ns, indicating membrane poration over that region.

performed taking two clusters simultaneously at different angular locations. Figure 4 shows the evolution of the TMP with two NP clusters placed across angular locations spanning the $9 < \theta < 18$ and $45 < \theta < 54$ regions. For consistency, the same seven angular locations over the spherical membrane as previously chosen were used for the TMP assessment. The $\theta = 18°$ and $\theta = 54°$ sites are predicted to be porated, while the other locations (including the $\theta = 9°$ angular position that is closest to the pole) remain intact. The results of Fig. 4 thus underscore the possibility of porating specific regions near NP clusters through suitable placements.
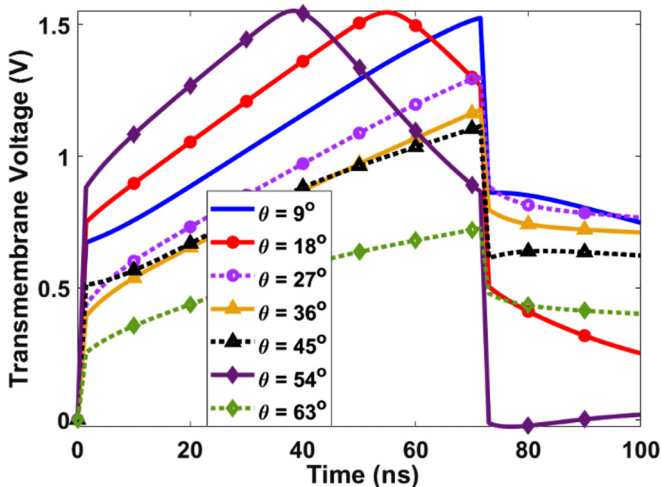

FIG. 4. Evolution of the TMP over time with two NP clusters placed over the angular locations spanning $9° < \theta < 18°$ and $45° < \theta < 54°$. For consistency, the same seven angular locations over the spherical membrane as in the previous figures are chosen. The $\theta = 18°$ and $\theta = 54°$ sites are predicted to be porated.

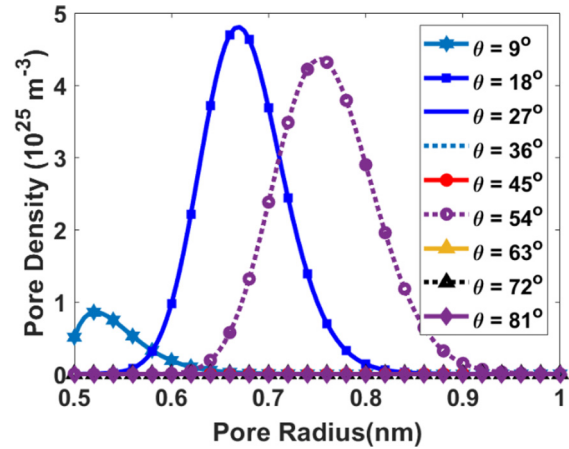FIG. 5. A 70-ns snapshot of the pore density distributions versus pore radius with two NPs placed at 9–18 ° and 45–54 ° as discussed in Fig. 4.

Our simulations also yielded the pore density distributions $n(r, t)$, at the various locations as a function of pore radius. A 70-ns snapshot of $n(r, t = 70\,\text{ns})$ versus pore radius [i.e., $n(r, t = 70\,\text{ns})$], with two NPs placed at 9–18 ° and 45–54 ° as previously discussed in Fig. 4 is shown in Fig. 5. The largest pores are predicted to occur at the 54 ° location, with a mean size of ∼0.75 nm. The pore distribution at the 18 ° location is smaller in size with a mean of ∼0.65 nm. Though the TMP was not predicted to decrease during the pulse application at the other locations in Fig. 4, the results of Fig. 5 do show a small rise in pores at the 9 ° location with an average radius of around 0.52 nm. This relatively small change, coupled with the small radius of pores at this location, was not seen to cause much alteration in the local membrane conductance. Hence, a practically unperturbed TMP resulted in Fig. 4 at this 9 ° position. All other locations in Fig. 5 showed no poration.

This possibility of porating multiple regions through the placement of multiple NPs was further tested by placing two NP clusters at other locations. Results for the time-dependent TMP with placements of two NP clusters over the location pairs spanning ($9° < \theta < 18°$ and $36° < \theta < 45°$), then ($9° < \theta < 18°$ and $54° < \theta < 63°$), and finally ($9° < \theta < 18°$ and $72° < \theta < 81°$) were obtained, and are shown collectively in Figs. 6(a)–6(c). For Fig. 6(a), the $\theta = 18°$ and $\theta = 45°$ locations are predicted to be porated; while the $\theta = 18°$ and $\theta = 63°$ sites can be seen to be porated in Fig. 6(b). In Fig. 6(c), the $\theta = 18°$ and $\theta = 81°$ locations are predicted to be porated. Thus, the two sets of NP clusters are shown to produce membrane porations at two locations each through local field enhancements. Details on the actual pore development are given in Fig. 6(d), which shows a 73-ns snapshot of the radial pore density distribution $n(r)$ vs r. Results at the four angular locations of 18 °, 45 °, 63 °, and 81 ° are given. Of these, the 45 ° point is predicted to have the largest pore sizes. The poration onset times of the membrane at the four sites at 45 °, 18 °, 63 °, and 81 ° were predicted to be 36.7, 53.6, 42.7, and 61.7 ns, respectively. In any event, the increase in pore density at all four locations underscore the positive role of the NPs in facilitating electroporation through local field enhancements.
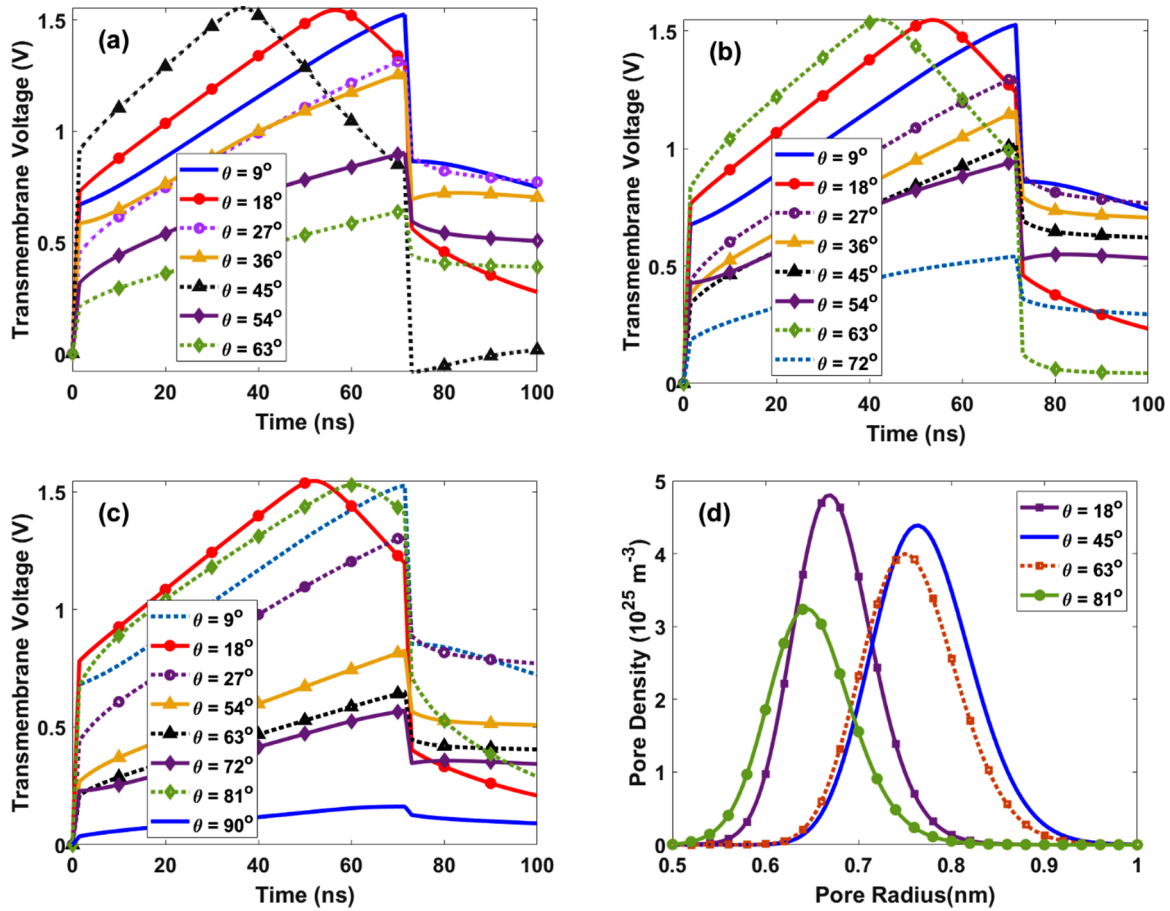
FIG. 6. Results for the dynamics with two NP clusters placed at different angular locations near the cell membrane. (a) Evolution of the TMP over time for NPs spanning $9° < \theta < 18°$ and $36° < \theta < 45°$, (b) TMP for NPs placed at the $9° < \theta < 18°$ and $54° < \theta < 63°$ angular positions, and (c) time-dependent TMP due to NPs spanning $9° < \theta < 18°$ and $72° < \theta < 81°$. (d) A 73-ns snapshot of the radial distribution $n(r)$ vs r for the pore densities at the four angular locations of $18°$, $45°$, $63°$, and $81°$.

Extending the calculations, results were next obtained for the TMP over time at different angular locations with three NP clusters, each placed at a separate position. Figure 7 shows the results for NP clusters spanning the zones of $9° < \theta < 18°$, and $45° < \theta < 54°$, and finally the $72° < \theta < 81°$ region. The results show that the $\theta = 18°$ and $\theta = 54°$ as well as the $\theta = 81°$ locations would all be porated after about 56, ~45, and ~54 ns, respectively, from the start of the electric pulse. A maximum voltage of ~1.5 V can be sustained in this case by the system. The important result is that the membrane at the $81°$ location is easily porated despite being close to the equatorial plane, with the event predicted to start slightly before the poration of the $18°$ segment. For completeness, simulation results were also obtained with two other three-NP cluster arrangements. In one set, the NPs were placed at 9–$18°$, 36–$45°$, and 72–$81°$. For the other, a combination spanning the regions from 9–$18°$, 54–$63°$, and 72–$81°$ was used. The results (not shown for brevity) revealed membrane poration in regions near the NP placement in all cases.

Results for the pore distributions $n(r, t)$ for three NP clusters placed at the locations spanning 9–$18°$, 54–$63°$, and 72–$81°$ are shown in Fig. 8. The following features emerge: (i) The largest pores are predicted to occur at the $81°$ location, with a mean size of ~0.75 nm. (ii) The pore distribution at the

$18°$ location has the highest amplitude with a mean radius of ~0.67 nm. (iii) The $63°$ location is seen to exhibit a profile

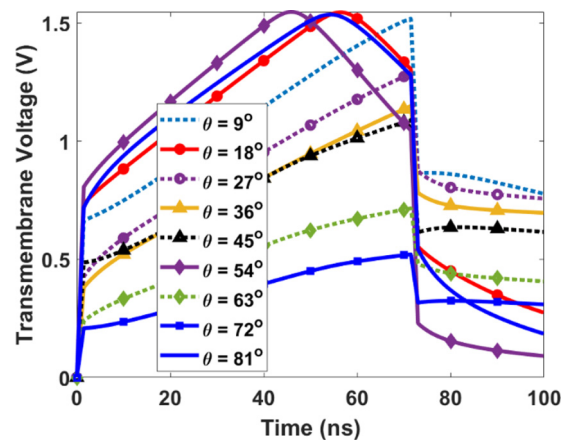FIG. 7. Results for the TMP over time at different angular locations with three NP clusters at angular locations spanning $9° < \theta < 18°$, $45° < \theta < 54°$, and finally $72° < \theta < 81°$. The $\theta = 18°$ and $\theta = 54°$ as well as the $\theta = 81°$ locations are all predicted to be porated at about 56, ~45, and ~54 ns, respectively.

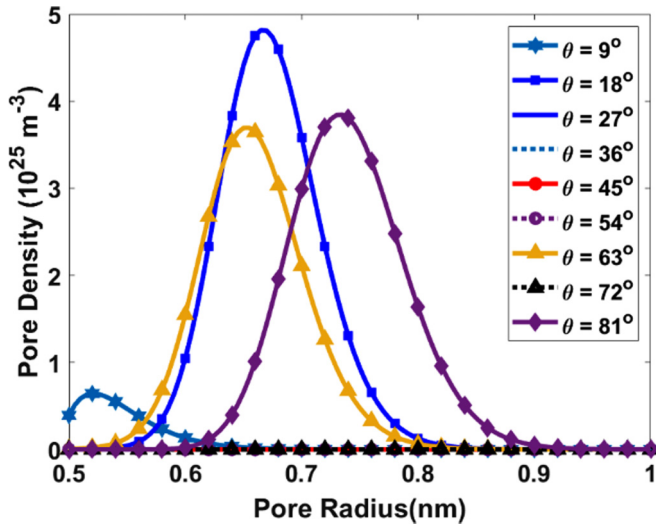FIG. 8. A 70-ns snapshot of the pore density distribution vs pore radius with three NPs placed at 9–18 °, 54–63 °, and 72–81 °.
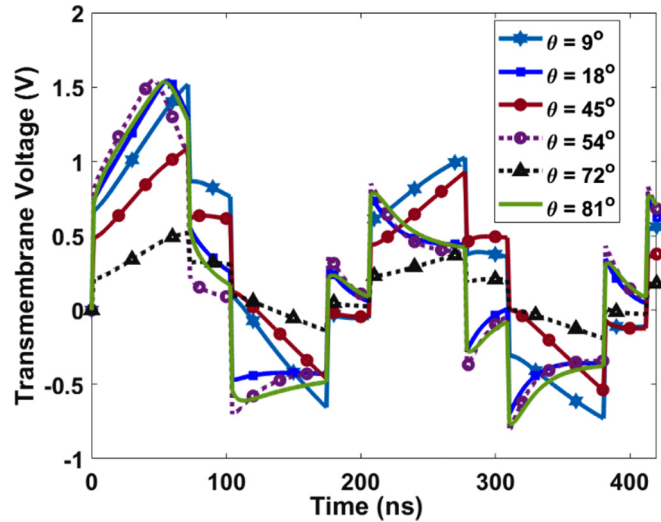

FIG. 9. Results for the TMP over time in response to a *bipolar pulse* at different angular locations with three NP clusters at angular locations spanning $9° < \theta < 18°$, $54° < \theta < 63°$, and $72° < \theta < 81°$. The $\theta = 54°$, $81°$, and $18°$ locations are all predicted to be porated at the first cycle.

similar to that at $81°$, but with the entire curve shifted to lower pore sizes, and an average of $\sim$0.63 nm. (iv) Though the region around the $9°$ angular location is seen to develop a small pore distribution, the radii are small. Hence, this would not be a likely site for electroporative-driven transport, with negligible consequence on the TMP. All other sites along the membrane probed through the calculations are predicted to remain unporated. (v) Finally, use of an elemental volume on the basis of the spherical grid implied the NP volume placed around the cell in the present simulations depended on $\sin(\theta)$, and so was progressively larger moving towards the equator at $\theta = 90°$. Hence, a larger volume of NPs was inherent with increasing angular position towards the equatorial plane. This suggests that nonuniform distributions would enable poration at regions further away from the poles. For completeness, it may be mentioned that for the pulse durations chosen, poration was only observed when NPs were included. This does not preclude the possibility of membrane poration with much longer duration pulses. However, for many applications, especially to remain within the nonthermal regime, it would still be useful to achieve NP-assisted electroporation quickly on these fast ($<$100 ns) time scales.

Finally for completeness, simulations were carried out for the time-dependent TMP in response to *bipolar excitation*. Such wave forms are already generating interest for tumor ablation applications using irreversible electroporation [49,50,97]. The bipolar pulse train was taken to have rise and fall times of 1.5 ns, a pulse ON time of 70 ns, and a pulse delay time of 30 ns. For easier comparison to the monopolar case, the geometry chosen was the one associated with Fig. 8 for three NP clusters spanning angular locations of 9–18 °, 54–63 °, and 72–81 °. The results given in Fig. 9 show the $\theta = 54°$, $81°$, and $18°$ locations to all be porated at the first cycle, which are close to the placement of the three individual NP clusters. The decrease in TMP magnitude during the reversal of the applied voltage persists at the $54°$, $81°$, and $18°$ locations, though the $54°$ and $81°$ locations exhibit greater changes over the 100–170-ns time span. The electroporation

is evident up to the third cycle starting around 412 ns. Due to poration, the peak amplitudes become progressively lower at 1.5, -0.7, $\sim$0.85, $\sim$$-0.73$, and $\sim$0.84 V. So roughly, the peak TMP for successive pulses after the initial exposure is predicted to stabilize at around $\sim$0.84 and $\sim$$-0.7$ V for the positive and negative polarities.

With a monopolar pulse train, a subsequent pulse can raise the TMP to an even higher level if the starting value (after a preceding pulse) were not to be at the zero level. For a bipolar pulse, on the other hand, if one is at a nonzero TMP value just prior to a subsequent pulse, the magnitude first goes through zero before being enhanced in the opposite direction. Consequently, the peak magnitude during the revered polarity does not become as large. Our results of Fig. 9 are in qualitative agreement with the above, and compare well with trends of previous experimental observations [98–100]. For instance, in the experiments by Gianulis *et al.* [98], the rate and amount of uptake for the marker dye YO-PRO-1 was consistently two- to threefold higher for unipolar pulses as compared to the bipolar treatments. A similar conclusion was reached by Roth *et al.* [99] and Sano and co-workers [100]. It is possible that the creation of pressure transients [99], or temperature gradients set up due to such electric pulse application [101] could alter the bioresponses in a synergistic manner. Though interesting, the latter will be analyzed and discussed elsewhere.

The corresponding pore density distribution [$= n(r, t)$] for this case of three NP clusters spanning angular locations of 9–18 °, 54–63 °, and 72–81 ° are shown in Fig. 10 for this bipolar excitation case. Figures 10(a) and 10(b) show snapshots at 176 and 412 ns, respectively. At both times, only the sites at the angular locations of $18°$, $54°$, $81°$, and $9°$ are predicted to be porated in that order with the largest magnitude at $18°$. Despite having the smallest density, the pores at $9°$ are predicted to evolve to the largest average radius of $\sim$1 nm at 412 ns. This implies that while this location closest to the pole
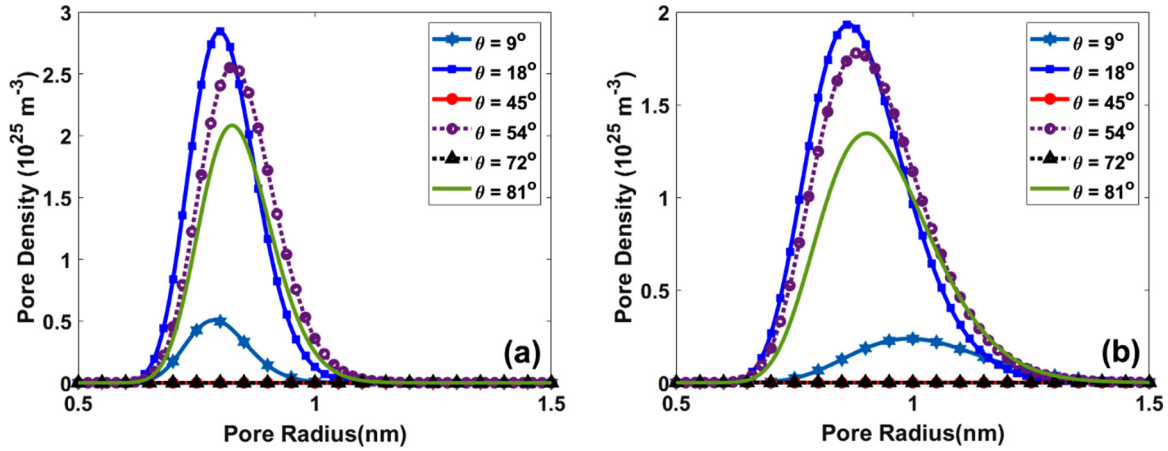
FIG. 10. Snapshots of the pore density distribution versus pore radius with three NPs placed over the regions spanning 9–18 °, 54–63 °, and 72–81 °, in response to a bipolar external electric field at (a) $T = 176$ ns and (b) $T = 412$ ns.

might not allow for a high inflow, the larger molecules could be accommodated by this site. Though longer simulations were not carried out, one might reasonably extrapolate to the possibility of stronger cellular uptake upon longer pulse trains as the pore radii could then keep increasing over time.

Overall, our simulation results are roughly in line with the experimental observations on electropermeabilization recently reported by Ghorbel *et al.* [77]. In their experiments, the use of platinum or gold NPs were shown to significantly increase the electroporative effect relative to the baseline case without NPs. The effects were seen to also depend on the proximity of the NPs from the cell membrane. Their data suggested that the plasma membrane was strongly influenced by the NP accumulation level around the cell membrane. For example, based on fluorescence data, it was shown that amplifying field strengths by having larger numbers of NPs could play an important role by increasing the size and/or number of membrane pores to boost the treatment efficiency, even for regions near the equatorial plane. In the simulations given here, this aspect of developing more electroporation sites through multiple NP placements near the membrane was affirmed. It was also demonstrated that regions far away from the polar axis could effectively be porated through the use of nanoparticles in their vicinity. Furthermore, our results demonstrate that nonuniform distributions would work to enable poration at regions further away from the poles.

It may also be mentioned that the results of Ghorbel *et al.* [77] were similar to other reports of enhanced cell electroporation using carbon nanotubes [102,103]. The similar outcomes from both carbon nanotubes and the spherical NPs used by the French group [77] suggest that the orientational effect of elongated NPs may not necessarily be as strong. In this connection, previous theoretical studies [104,105] had suggested that elongated microconductors would be better at producing local field enhancements to promote electroporation. However, the separation distance was not probed, and analytic expressions for field enhancement factors indicate a quick falloff with increasing distance from a NP [104,106–108]. For example, a simple treatment which replaces the metallic spheroid by an equivalent line charge lying sym-

metrically about the origin [109,110] can yield the electric fields in analytic form. The electric field $E_z(z, r)$ at any axial and radial locations "z" and "r" can be obtained based on a simple integration of the charge distribution, and leads to the following expression:

$$E_z(z, 0) = -\int_0^h \frac{\tau z' dz'}{4\pi \varepsilon (z - z')^2} - \int_{-h}^0 \frac{\tau z' dz'}{4\pi \varepsilon (z - z')^2}. \quad (2)$$

Carrying out the integration yields

$$E_z(z, 0) = -E_0 \left(1 + \frac{\frac{2ecz}{z^2 - e^2 c^2} - \ln\left(\frac{z + ec}{z - ec}\right)}{\ln\left(\frac{1 + e}{1 - e}\right) - 2e} \right), \quad (3)$$

where E_0 represents the externally applied electric field, $h = ec$, where e is the eccentricity defined in terms of the semimajor "c" and semiminor axes "a" as e $= [1 - (a/c)^2]^{1/2}$, and $\tau/(4\pi \varepsilon) = E_0/\{\ln[(1 + e)/(1 - e)] - 2e\}$, with ε the permittivity. For a sphere with $e = 0$, the field at the poles (i.e., $z = c$) works out to $E_z(z = c, 0) = -3E_0$. However, in the presence of a membrane dielectric, the above simple results would not apply. Formulations suggested by Lehner [104] or Smythe [111] could be simple extensions. In the present analysis, though, a more complete description of a multicomponent system with details pertaining to the material properties of the bilipid membrane, surrounding water, etc., have naturally been folded in.

A final comment in this regard pertains to the subtle difference between membrane poration (as discussed here) and mass transport through cells which is often referred to as permeabilization and is the ultimate desired outcome. These are basically two different phenomena that occur on different time scales and are governed by distinct processes. Pore creation involves short-term dynamics, while permeabilization of the lipid bilayer is a long-term phenomenon. This splitting is necessary to account for experimental results that at first glance might seem contradictory. On the one hand, for example, the observations of Benz *et al.* [112] and molecular dynamics (MD) simulations [93,113] show that pores shrink within a few microseconds (or tens of nanoseconds for MD simulations) after external pulsing is turned off. On the other hand, it has been reported that the permeable state of a membrane can

last several minutes after the pulse delivery [114,115]. Unfortunately, however, a clear understanding of the processes and underlying reasons for this distinction remains elusive. While lipid peroxidation has been suggested as a possible mechanism for the prolonged membrane permeabilization [116], experiments by Michel *et al.* [117] concluded that while lipid oxidation can occur at the plasma membrane after electric pulsing, it could not be the cause of long-lasting membrane permeabilization. In any case, regardless of the mechanistic details, the mere presence of heightened electric fields via the use of NPs remains an important driver for several secondary bioeffects and merits further analysis.

IV. CONCLUSIONS

Electroporation is a useful technique for cellular biomanipulation, drug and gene delivery, and for targeted apoptosis. An important practical consideration is the ease of throughput and delivery into cells (and tissues), or the applications to tumor ablation using irreversible electroporation that could be optimized. The use of NPs is known to provide a step in this direction, and the relevant analysis was presented and discussed in this contribution. The role of the NPs in modifying and enhancing the TMP was probed with regard to the position and placement of the nanoparticle clusters. The results from the time-evolving TMP were then fed into a continuum Smoluchowski equation [73–75] for analysis of pore formation and growth. Comparisons were also made between monopolar and bipolar pulse responses.

The results showed strong increases in TMP in the presence of NP clusters near the cell membrane. The results clearly demonstrated that it is indeed possible to quickly porate regions of the membrane, increase the fractional area of the cells over which poration could take place, and influence locations lying far away from the poles. For the pulse durations chosen, the poration was only observed when NPs were included. This does not preclude the possibility of membrane poration with much longer duration pulses. However, for many applications, especially within the nonthermal regime, it would still be useful to achieve NP-assisted electroporation on the faster (<100 ns) time scales. The use of NPs could thus act as distributed electrodes capable of enhancing the cellular

inflows through electroporation tailored by fields at the desired locations. This trend was shown to hold for both unipolar and bipolar pulses. From the bipolar simulation results, it might seem possible to even tailor the inflow of different sized molecules from different locations around a cell through NP placements, and that stronger cellular uptake could result from longer pulse trains.

The present simulation results were roughly in line with the experimental observations reported by Ghorbel *et al.* [77]. The aspect of developing more electroporation sites or affecting larger areas of the membrane surface through multiple NP placements near the membrane was affirmed. It is conceivable that in cases where the external field strength are not too large, the amplification provided by having a larger number of NPs could play an important role by increasing the size and/or number of membrane pores to boost cellular intake. Our results do demonstrate that nonuniform distributions would work to enable poration at regions that were further away from the poles. Since the field amplification is dependent on the distance from the membrane, close placement of NP clusters would likely be necessary. Anisotropic geometries could further boost the field enhancements created by the NPs (especially at small separations under 10 nm) and would be studied elsewhere. Other effects of relevance to membrane poration and cellular transport such as localized heating by external excitation [101,118] for synergistic effects could also be analyzed using the present technique and will be probed elsewhere. Finally, since transmembrane potential patterns have been shown to play a regulatory role in development and regeneration [119], it is conceivable that such externally controlled TMP manipulations and NP-based electric treatments could influence embryogenesis [120,121] and/or wound healing [122].

The data that support the findings of this study are available from the corresponding author upon reasonable request.

ACKNOWLEDGMENTS

[1] U. Zimmermann, Biochim. Biophys. Acta, Rev. Biomembr. **694**, 227 (1982).

[2] C. A. Jordan, E. Neumann, and A. E. Sowers, in *Electroporation and Electrofusion in Cell Biology* (Springer Science and Business Media, New York, 2013).

[3] W. Arnold and U. Zimmermann, Biol. Membr. **5**, 389 (1984).

[4] G. Fuhr, R. Glaser, and R. Hagedorn, Biophys. J. **49**, 395 (1986).

[5] H. A. Pohl and J. S. Crane, Biophys. J. **11**, 711 (1971).

[6] F. A. Sauer, Forces on suspended particles in the electromagnetic field, in *Coherent Excitations in Biological Systems* (Springer, New York, 1983), pp. 134–144.

[7] F. F. Becker, X.-B. Wang, Y. Huang, R. Pethig, J. Vykoukal, and P. Gascoyne, Proc. Natl. Acad. Sci. **92**, 860 (1995).

[8] P. R. Gascoyne and J. Vykoukal, Electrophoresis **23**, 1973 (2002).

[9] E. Neumann and K. Rosenheck, J. Membr. Biol. **10**, 279 (1972).

[10] R. Stampfli, An. Acad. Bras. Cienc. **30**, 57 (1958).

[11] T. Y. Tsong, Biophys. J. **60**, 297 (1991).

[12] J. C. Weaver and Y. A. Chizmadzhev, Bioelectrochem. Bioenerg. **41**, 135 (1996).

[13] I. G. Abidor, V. B. Arakelian, Y. Chemomordik, A. Chizmadzhev, V. F. Pastushenko, and M. R. Tarasevich, Bioelectrochem. Bioenerg. **6**, 37 (1979).

[14] S. H. Meglic and T. Kotnick, Electroporation-based applications in biotechnology, in *Handbook of Electroporation*, edited by D. Miclavčič (Springer International, Cham, Switzerland, 2016), pp. 2153–2169.

[15] R. P. Joshi and K. H. Schoenbach, Crit. Rev. Bio-Med. Eng. **38**, 255 (2010).

[16] M. P. Rols and J. Teissie, Biophys. J. **65**, 409 (1998).

[17] J. A. Nollet, *Recherches sur les Causes Particulieres des Phenomenes Electriques* (Guerin and Delatour, Paris, 1754).

[18] E. Neumann, M. Schaefer-Ridder, Y. Wang, and P. H. Hofschneider, EMBO J. **1**, 841 (1982).

[19] A. Gothelf and J. Gehl, Curr. Gene Ther. **10**, 287 (2010).

[20] H. Aihara and J. Miyazaki, Nat. Biotechnol. **16**, 867 (1998).

[21] A. I. Daud, R. C. DeConti, S. Andrews, P. Urbas, A. I. Riker, V. K. Sondak, P. N. Munster, D. M. Sullivan, K. E. Ugen, J. L. Messina, and R. Heller, J. Clin. Oncol. **26**, 5896 (2008).

[22] A. V. Titomirov, S. Sukharev, and E. Kistanova, Biochim. Biophys. Acta **1088**, 131 (1991).

[23] F. M. André, J. Gehl, G. Sersa, V. Préat, P. Hojman, J. Eriksen, M. Golzio, M. Cemazar, N. Pavselj, M.-P. Rols, D. Miklavčič, E. Neumann, J. Teissié, and L. M. Mir, Hum. Gene Ther. **19**, 1261 (2008).

[24] C. Rosazza, S. H. Meglic, A. Zumbusch, M. P. Rols, and D. Miklavčič, Curr. Gene Ther. **16**, 98 (2016).

[25] L. Heller and R. Heller, Hum. Gene Ther. **17**, 890 (2006).

[26] L. M. Mir, M. Belehradek, C. Domenge, S. Orlowski, B. Poddevin, J. Belehradek, Jr., G. Schwaab, B. Luboinski, and C. Paoletti, C. R. Acad. Sci. III **313**, 613 (1991).

[27] D. Miklavčič, B. Mali, B. Kos, R. Heller, and G. Serša, BioMed. Eng. OnLine **13**, 29 (2014).

[28] M. R. Prausnitz, V. G. Bose, R. Langer, and J. C. Weaver, Proc. Natl. Acad. Sci. USA **90**, 10504 (1993).

[29] M. L. Yarmush, A. Golberg, G. Sersa, T. Kotnik, and D. Miklavčič, Annu. Rev. Biomed. Eng. **16**, 295 (2014).

[30] R. Nuccitelli, J. C. Berridge, Z. Mallon, M. Kreis, B. Athos, and P. Nuccitelli, PLoS One **10**, e0134364 (2015).

[31] C. Y. Calvet and L. M. Mir, Cancer Metastasis Rev. **35**, 165 (2016).

[32] G. Sersa, J. Teissie, M. Cemazar, E. Signori, U. Kamensek, G. Marshal, and D. Miklavčič, Cancer Immunol. Immunother. **64**, 1315 (2015).

[33] M. Marty, G. Sersa, J. R. Garbay, J. Gehl, C. G. Collins, M. Snoj, V. Billard, P. F. Geerrtsen, J. O. Larkin, D. Miklavčič, I. Pavlovic, S. M. Paulin-Kosir, M. Cemazar, N. Morsli, D. M. Soden, Z. Rudolf, C. Robert, G. C. O'Sullivan, and L. M. Mir, Eur. J. Cancer Suppl. **4**, 3 (2006).

[34] M.Cemazar and G. Sersa, Bioelectricity **1**, 204 (2019).

[35] G. Schmidt, I. Juhasz-Böss, E.-F. Solomayer, and D. Herr, Geburtshilfe Frauenheilkd. **74**, 557 (2014).

[36] G. Pucihar, T. Kotnik, M. Kandušer, and D. Miklavčič, Bioelectrochemistry **54**, 107 (2001).

[37] L. Low, A. Mander, K. McCann, D. Dearnaley, T. Tjelle, I. Mathisen, F. Stevenson, and C. H. Ottensmeier, Hum. Gene Ther. **20**, 1269 (2009).

[38] C. Y. Calvet, F. M. André, and L. M. Mir, Oncoimmunology **3**, e28540 (2014).

[39] R. P. Joshi and K. H. Schoenbach, Electric fields in biological cell and membranes, in *Electromagnetic Fields in Biological Systems*(CRC, Boca Raton, FL, 2011), pp. 71–114.

[40] T. B. Napotnik, M. Reberšek, P. T. Vernier, B. Mali, and D. Miklavčič, Bioelectrochemistry **110**, 1 (2016).

[41] S. J. Beebe, P. F. Blackmore, J. White, R. P. Joshi and K. H. Schoenbach, Physiol. Meas. **25**, 1077 (2004).

[42] M. R. Cho, H. S. Thatte, M. T. Silvia, and D. E. Golan, FASEB J. **13**, 677 (1999).

[43] R. Nuccitelli, U. Pliquett, X. Chen, W. Ford, R. J. Swanson, S. J. Beebe, J. F. Kolb, and K. H. Schoenbach, Biochem. Biophys. Res. Commun. **343**, 351 (2006).

[44] R. Nuccitelli, R. Wood, M. Kreis, B. Athos, J. Huynh, K. Liu, P. Nuccitelli, and E. H. Epstein, Exp. Dermatol. **23**, 135 (2014).

[45] R. P. Joshi, A. Mishra, J. Song, A. Pakhomov, and K. H. Schoenbach, IEEE Trans. Biomed. Eng. **55**, 1391 (2008).

[46] K. H. Schoenbach, B. Hargrave, R. P. Joshi, J. F. Kolb, R. Nuccitelli, C. Osgood, A. Pakhomov, M. Stacey, R. J. Swanson, J. White, S. Xiao, J. Zhang, S. J. Beebe, P. F. Blackmore, and E. S. Buescher, IEEE Trans. Dielectr. Electr. Insul. **14**, 1088 (2007).

[47] N. Jourabchi, K. Beroukhim, B. A. Tafti, S. T. Kee, and E. W. Lee, Gastrointest. Intervention **3**, 8 (2014).

[48] M. Ahmed, C. L. Brace, F. T. Lee Jr., and S. N. Goldberg, Radiology **258**, 351 (2011).

[49] M. B. Sano, C. B. Arena, K. R. Bittleman, M. R. DeWitt, H. J. Cho, C. S. Szot, D. Saur, J. M. Cissel, J. Robertson, Y. W. Lee, and R. V. Davalos, Sci. Rep. **5**, 14999 (2015).

[50] E. L. Latouche, C. B. Arena, J. W. Ivey, P. A. Garcia, T. E. Pancotto, N. Pavlisko, S. S. Verbridge, R. V. Davalos, and J. H. Rossmeisl, Technol. Cancer Res. Treat. **17**, 1 (2018).

[51] J. F. Edd, L. Horowitz, R. V. Davalos, L. M. Mir, and B. Rubinsky, IEEE Trans. Biomed. Eng. **53**, 1409 (2006).

[52] L. G. Campana, M. Cesari, F. Dughiero, M. Forzan, M. Rastrelli, C. R. Rossi, E. Sieni, and A. L. Tosi, Med. Biol. Eng. Comput. **54**, 773 (2016).

[53] T. García-Sánchez, R. Bragós, and L. M. Mir, Biosens. Bioelectron. **117**, 207 (2018).

[54] J. W. Loomis-Husselbee, P. J. Cullen, R. F. Irvine, and A. P. Dawson, Biochem. J. **277**, 883 (1991).

[55] S. A. A. Kooijmans, S. Stremersch, K. Braeckmans, S. C. De Smedt, A. Hendrix, M. J. A. Wood, R. M. Schiffelers, K. Raemdonck, and P. Vader, J. Controlled Release **172**, 229 (2013).

[56] R. Stapulionis, Bioelectrochem. Bioenerg. **48**, 249 (1999).

[57] B Ferraro, L. C. Heller, Y. L. Cruz, S. Guo, A. Donate, and R. Heller, Gene Ther. **18**, 496 (2011).

[58] G. Sersa, M. Cemazar, D. Semrov, and D. Miklavčič, Bioelectrochem. Bioenerg. **39**, 61 (1996).

[59] R. A. Gilbert, M. J. Jaroszeski, and R. Heller, Biochim. Biophys. Acta **1334**, 9 (1997).

[60] C. Faurie, E. Phez, M. Golzio, C. Vossen, J. C. Lesbordes, C. Delteil, J. Teissie, and M. P. Rols, Biochim. Biophys. Acta **1665**, 92 (2004).

[61] Y. Zu, S. Huang, W. C. Liao, Y. Lu, and S. Wang, J. Biomed. Nanotechnol. **10**, 982 (2014).

[62] M. M. Mahan and A. L. Doiron, J. Nanomater. **2018**, 5837276 (2018).

[63] M. A. Busquets, J. Estelrich, and M. J. Sánchez-Martín, Int. J. Nanomed. **140**, 1727 (2015).

[64] S. C. Baetke, T. Lammers, and F. Kiessling, Br. J. Radiol. **88**, 20150207 (2015).

[65] J. F. Hainfeld, D. N. Slatkin, and H. M. Smilowitz, Phys. Med. Biol. **49**, N309 (2004).

[66] D. Jaque, L. Martínez Maestro, B. del Rosal, P. Haro-Gonzalez, A. Benayas, J. L. Plaza, E. Martín Rodríguez, and J. G. Solé, Nanoscale **6**, 9494 (2014).

[67] D. Miklavčič, V. Novickij, M. Kranj, T. Polajzer, S. H. Meglic, T. Batista Napotnik, R. Romih, and D. Lisjak, Bioelectrochemistry **132**, 107440 (2019).

[68] S. Gelperina, K. Kisich, M. D. Iseman, and L. Heifets, Am. J. Respir. Crit. Care Med. **172**, 1487 (2005).

[69] V. V. Mody, A. Cox, S. Shah, A. Singh, W. Bevins, and H. Parihar, Appl. Nanosci. **4**, 385 (2014).

[70] A. Ghorbel, F. M. André, L. M. Mir, and T. García-Sánchez, Bioelectrochemistry **137**, 107642 (2021).

[71] R. P. Joshi, Q. Hu, and K. H. Schoenbach, IEEE Trans. Plasma Science **32**, 1677 (2004).

[72] R. P. Joshi and Q. Hu, Med. Biol. Eng. Comput. **48**, 837 (2010).

[73] S. B. Dev, D. Dhar, and W. Krassowska, IEEE Trans. Biomed. Eng. **50**, 1296 (2003).

[74] J. C. Neu and W. Krassowska, Phys. Rev. E **59**, 3471 (1999).

[75] R. P. Joshi and K. H. Schoenbach, Phys. Rev. E **62**, 1025 (2000).

[76] D. Miklavčič, V. Novickij, M. Kranjc, T. Polajzer, S. H. Meglic, T. Batista Napotnik, R. Romih, and D. Lisjak, Bioelectrochemistry **132**, 107440 (2020).

[77] A. Ghorbel, L. M. Mir, and T. García-Sánchez, Nanotechnology **30**, 495101 (2019).

[78] Z. Vasilkoski, A. T. Esser, T. R. Gowrishankar, and J. C. Weaver, Phys. Rev. E **74**, 021904 (2006).

[79] K. C. Melikov, V. A. Frolov, A. Shcherbakov, A. V. Samsonov, Y. A. Chizmadzhev, and L. V. Chernomordik, Biophys. J. **80**, 1829 (2001).

[80] M. Essone Mezeme, G. Pucihar, M. Pavlin, C. Brosseau, and D. Miklavčič, Appl. Phys. Lett. **100**, 143701 (2012).

[81] E. Gongadze, A. Velikonja, S. Perutkova, P. Kramar, A. Maček-Lebar, V. Kralj-Iglič, and A. Iglič, Electrochim. Acta **126**, 42 (2014).

[82] A. Velikonja, S. Perutkova, E. Gongadze, P. Kramar, A. Polak, A. Maček-Lebar, and A. Iglič, Int. J. Mol. Sci. **14**, 2846 (2013).

[83] R. P. Joshi, J. Qian, K. H. Schoenbach, and E. Schamiloglu, J. Appl. Phys. **96**, 3617 (2004).

[84] A. Barnett and J. C. Weaver, Bioelectrochem. Bioenerg. **25**, 163 (1991).

[85] V. F. Pastushenko and Yu A. Chhizmadzhev, Biofizika **27**, 475 (1982).

[86] S. A. Freeman, M. A. Wang, and J. C. Weaver, Biophys. J. **67**, 42 (1994).

[87] R. W. Glaser, S. L. Leikin, L. V. Chernomordik, V. F. Pastushenko, and A. I. Sokirko, Biochim. Biophys. Acta **940**, 275 (1988).

[88] M. Smoluchowski, Phys. Z. **17**, 557 (1916).

[89] S. Chandrasekhar, Rev. Mod. Phys. **15**, 1 (1943).

[90] H. A. Kramers, Physica **7**, 284 (1940).

[91] Q. Hu and R. P. Joshi, J. Appl. Phys. **122**, 034701 (2017).

[92] M. Tarek, Biophys. J. **88**, 4045 (2005).

[93] Q. Hu, Z. Zhang, H. Qiu, M. G. Kong, and R. P. Joshi, Phys. Rev. E **87**, 032704 (2013).

[94] Q. Hu, R. P. Joshi, and K. H. Schoenbach, Phys. Rev. E **72**, 031902 (2005).

[95] P. T. Vernier, Y. Sun, L. Marcu, S. Salemi, C. M. Craft, and M. A. Gundersen, Biochem. Biophys. Res. Commun. **310**, 286 (2003).

[96] K. H. Schoenbach, R. P. Joshi, J. Kolb, N. Chen, M. Stacey, P. Blackmore, E. S. Buescher, and S. J. Beebe, Proc. IEEE **92**, 1122 (2004).

[97] R. V. Davalos, L. M. Mir, and B. Rubinsky, Ann. Biomed. Eng. **33**, 223 (2005).

[98] E. C. Gianulis, J. Lee, C. Jiang, S. Xiao, B. L. Ibey, and A. G. Pakhomov, Sci. Rep. **5**, 13818 (2015).

[99] C. C. Roth, R. A. Barnes, Jr., B. L. Ibey, H. T. Beier, L. C. Mimun, S. M. Maswadi, M. Shadaram, and R. D. Glickman, Sci. Rep. **5**, 15063 (2015).

[100] M. B. Sano, C. B. Arena, M. R. DeWitt, D. Saur, and R. V. Davalos, Bioelectrochemistry **100**, 69 (2014).

[101] J. Song, A. L. Garner, and R. P. Joshi, Phys. Rev. Appl. **7**, 024003 (2017).

[102] V. Raffa, G. Ciofani, O. Vittorio, V. Pensabene, and A. Cuschieri, Bioelectrochemistry **79**, 136 (2010).

[103] L. Wang, D. Liu, R. Zhou, Z. Wang, and A. Cuschieri, Int. J. Mol. Sci. **16**, 6890 (2015).

[104] J. Lekner, Phys. Med. Biol. **59**, 6031 (2014).

[105] H. Qiu, R. P. Joshi, and A. K. Pradhan, J. Appl. Phys. **116**, 184701 (2014).

[106] E. G. Pogorelov, A. I. Zhbanov, and Y. C. Chang, Ultramicroscopy **109**, 373 (2009).

[107] V. Q. Huynh, B. Techaumnat, and K. Hidaka, IEEE Trans. Dielectr. Electr. Insula. **20**, 2230 (2013).

[108] P. I. Geshev, S. Klein, T. Witting, K. Dickmann, and M. Hietschold, Phys. Rev. B **70**, 075402 (2004).

[109] A. E. DePrince and R. J. Hinde, Nanoscale Res. Lett. **5**, 592 (2010).

[110] B. Techaumnat and M. Washizu, J. Electrost. **69**, 388 (2011).

[111] W. R. Smythe, *Static and Dynamic Electricity* (McGraw-Hill, New York, 1950).

[112] R. Benz, F. Beckers, and U. Zimmermann, J. Membr. Biol. **48**, 181 (1979).

[113] L. Delemotte and M. Tarek, J. Membrane Biol. **245**, 531 (2012).

[114] M. Rols, C. Delteil, M. Golzio, and J. Teissié, Eur. J. Biochem. **254**, 382 (1998).

[115] J. Teissié, and C. Ramos, Biophys. J. **74**, 1889 (1998).

[116] L Rems, M. Viano, M. A. Kasimova, D. Miklavčič, and M. Tarek, Bioelectrochemistry **125**, 46 (2019).

[117] O. Michel, A. G. Pakhomov, M. Casciola, J. Saczko, J. Kulbacka, and O. N. Pakhomova, Bioelectrochemistry **132**, 107433 (2020).

[118] V. Pierro, A. De Vita, R. P. Croce, and I. M. Pinto, IEEE Trans. Plasma Sci. **42**, 2236 (2014).

[119] M. Levin, G. Pezzulo, and J. M. Finkelstein, Annu. Rev. Biomed. Eng. **19**, 353 (2017).

[120] K. B. Hotary and K. R. Robinson, Development **114**, 985 (1992).

[121] M. Levin, in *The physiology of bioelectricity in development, tissue regeneration and cancer*, edited by C. E. Pullar (CRC Press, Boca Raton, 2016), Chap. 3, pp. 39–90.

[122] B. Reid and M. Zhao, Adv. Wound Care **3**, 184 (2014).